NUMERICAL INVESTIGATION OF PLUNGING DENSITY CURRENT

By P. E. Bournet,[1] D. Dartus,[2] B. Tassin,[3] and B. Vinçon-Leite[4]

ABSTRACT: When a buoyant inflow of higher density enters a reservoir, it sinks below the ambient water and forms an underflow. Downstream of the plunge point, the flow becomes progressively diluted due to the fluid entrainment. The entrainment rate is strongly dependent on the Richardson number and reaches a constant value well downstream of the plunge point. This study is concerned with the analysis of the plunging phenomenon and the determination of the entrainment. A k-ε model including buoyancy effects, both in a sloping and a diverging channel, is used to reproduce the main flow characteristics. A relation between the depth at the plunge point in a channel of constant width and in a diverging channel is established, and theoretical results for the calculation of the dense layer thickness are provided. The latter indicates that the spreading rate of the dense layer in a diverging channel is a function of both the entrainment rate and the channel width. The predictions of the plunge line location are in agreement with most semiempirical equations.

INTRODUCTION

When a river enters the relatively quiescent water of a lake or reservoir, it meets waters of slightly different temperature, salinity, or turbidity. Three configurations may occur. First, if the river is lighter than the surface water, it will form an overflow. Such a current has been observed in Lake Kootenay in Canada (Carmack et al. 1986). Second, if the river reaches a depth where its density equals that of the ambient lake water, the plume separates from the bottom and spreads horizontally along surfaces of constant density (Hamblin and Carmack 1978). Third, when the river is heavier than the water of the lake, it sinks and flows as an inclined plume along its morphological channel. For instance, such a current has been reported by Hebbert et al. (1979) in the Wellington Reservoir in Australia.

The analysis of density currents is of great relevance for water quality management in reservoirs as they carry suspended matters and dissolved solids across the lake. Consequently, density currents often determine the distribution of pollutant substances in lakes. Furthermore, information on inflow behavior is needed as input to 1D unsteady water quality models of stratified reservoirs and lakes.

Density currents have been observed in situ (Serruya 1974; Smith 1975; Carmack et al. 1979; Fischer and Smith 1983; Alavian and Ostrowski 1992; Chikita 1992) and in the laboratory (Akiyama and Stefan 1984; Hauenstein and Dracos 1984; Alavian 1986; Stefan et al. 1988). Previous studies have essentially dealt with inclined channels of constant width (Singh and Shah 1971; Savage and Brimberg 1975; Denton 1985; Kranenburg 1993). Most of these authors have coupled experimental approaches to semiempirical analyses. They have advanced semiempirical relations for the depth at the plunge point. Others used a 2D hydrodynamic model considering that the channel had a triangular shape and assuming that the density current did not participate in the dynamics of heating and mixing but that entrainment from the ambient reservoir into the downflow took place (Imberger and Patterson 1981; Buchak and Edinger 1984; Jokela and Patterson 1985). Recently, some authors have considered channels of variable widths (Akiyama and Stefan 1987; Johnson et al. 1987; Stefan et al. 1988) or unbounded 3D plumes (Hauenstein and Dracos 1984; Alavian 1986; Alavian et al. 1992), but few authors have considered the problem by solving the whole set of the Navier-Stokes equations using the buoyancy-extended k-ε closure (Farrell and Stefan 1986; Sini 1986; Fukushima and Watanabe 1990).

The present study is limited to currents with a density higher than the density of the ambient water in the lake. The aim is to investigate the spread of turbulent density currents generated by inflows into stagnant generally homogeneous ambient water. In this paper, the modified k-ε model with buoyancy effects is used to describe the characteristics of density currents in terms of plunge point and entrainment in an inclined channel of constant width and then in a diverging channel. On the basis of the numerical results, calculations of the entrainment as well as of the plunge line will be achieved and compared with semiempirical models of the literature.

Two cases are successively considered: (1) An inclined channel of constant width; and (2) an inclined diverging channel that constitutes the most usual case of a river entering a lake.

PROCESSES AND EMPIRICAL MODEL OF PLUNGING DENSITY CURRENT

Plunge Concept

Density currents consist of two regions of steady flow: (1) a momentum dominated region; and (2) a buoyancy dominated region. At a position determined by a balance between the momentum of the inflow and the baroclinic pressure resulting from the density difference between the inflow and the receiving water, the inflow may form an overflow, or plunge below the surface. Beyond the plunge point, a two-layer flow occurs and mixing across the density interface as well as dilution of the underflow take place. This process is called entrainment. The flow initially consists of a bottom density current that spreads down a slope. After the head of the current has passed, the undercurrent reaches steady state. Because of the shear developed at the interface between the underflow and the overlying reservoir water, a slow recirculating flow is set up in the overlying reservoir such that the surface water moves toward the plunge line. The surface of separation is governed by two driving forces and one resisting force. The driving forces are the dynamic force exerted by the stream due to its higher momentum and the static force due to the pressure gra-

[1]Res., Centre d'Enseignement et de Recherche pour la Gestion des REssources Naturelles et de l'Environnement, 77455 Marne la Vallée cedex 2, France.

[2]Lect., Institut de Mécanique des Fluides de Toulouse, 31400 Toulouse, France.

[3]Res., Centre d'Enseignement et de Recherche pour la Gestion des REssources Naturelles et de l'Environnement, 77455 Marne la Vallée cedex 2, France.

[4]Res., Centre d'Enseignement et de Recherche pour la Gestion des REssources Naturelles et de l'Environnement, 77455 Marne la Vallée cedex 2, France.

Note. Discussion open until November 1, 1999. To extend the closing date one month, a written request must be filed with the ASCE Manager of Journals. The manuscript for this paper was submitted for review and possible publication on February 9, 1996. This paper is part of the ***Journal of Hydraulic Engineering***, Vol. 125, No. 6, June, 1999. ©ASCE, ISSN 0733-9429/99/0006-0584–0594/$8.00 + $.50 per page. Paper No. 12605.

dient across the surface of separation. The shear stresses along the surface of separation and the bed provide the resisting force. The net effect of these forces determines the shape and the movement of the surface of separation. The stable position is achieved when the forces are balanced.

Plunge Depth for Channel of Constant Width

Physical parameters controlling plunging depend on inflow conditions as well as the geometrical characteristics of the reservoir (Fig. 1). The parameters are inflow per unit width upstream q_0, the ambient fluid density ρ_a, the inflow fluid density $\rho_0 = \rho_a + \Delta\rho_0$, the acceleration of gravity g, the inflow depth h_0, the total friction coefficient of the underflow C_D, the bottom slope $S = \tan\theta$, and the initial mixing coefficient γ. γ is defined as the ratio of the amount of ambient reservoir water entrained at the plunge point to the inflowing river discharge. Dimensional analysis gives the normalized plunge depth h_p/h_0, where h_p = depth of plunging, and h_0 = depth of inflow channel, as a function of the above mentioned parameters (Akiyama and Stefan 1984)

$$\frac{h_p}{h_0} = f\left[\left(\frac{q_0^2}{\varepsilon_0 g h_0^3}\right)^{1/3}, S, C_D, \gamma\right] \tag{1}$$

where ε_0 = relative density difference between inflow and ambient water $\varepsilon_0 = \Delta\rho_0/\rho_a$.

From laboratory experiments, Singh and Shah (1971) established an empirical correlation between the depth at the plunge point and initial flow and density difference conditions. Savage and Brimberg (1975) presented two analyses of the plunging plume phenomenon: The former is based on a simple energy flow conservation analysis, and the latter on the analysis of a gradually varied two-layer flow. They obtained relations for the depth at the plunge point as well as for various types of interfacial profiles from an analysis similar to that of the hydraulic jump. Akiyama and Stefan (1984) proposed a synthesis

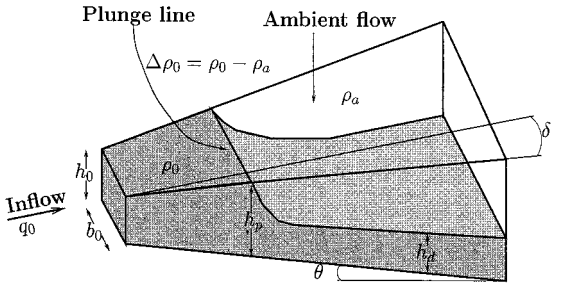

FIG. 1. Definition Sketch of Relevant Parameters for Diverging Channel with Sloping Bottom

of the equations for the plunge depth and established relations taking into account the slope as well as the dilution and friction coefficient. Stefan et al. (1988) analyzed the plunging phenomenon in terms of densimetric Froude number which is dependent on the slope and the friction coefficient.

Table 1 is a summary of the different semiempirical relations found in the literature. They can be expressed in the general form

$$h_p = \left(\frac{1}{F_p^2}\right)^{1/3}\left(\frac{q_0^2}{\varepsilon_0 g}\right)^{1/3} \tag{2}$$

where F_p = densimetric Froude number at the plunge point that is often empirically determined.

For channels of constant width, various authors have found values of F_p within the range $0.1 < F_p < 0.9$ for slopes varying between $10^{-3} < S < 0.25$ [see Akiyama and Stefan (1987) and Alavian et al. (1992)], with a mean value of $F_p = 0.57$.

Plunge Depth for Horizontal Diverging Channel

Few authors have considered the 3D aspects of an unbounded density current (Hauenstein and Dracos 1984; Alavian 1986), or the spread of an underflow is a diverging channel (diffuser) (Johnson et al. 1987, 1989; Alavian et al. 1992). In most lakes and reservoirs, however, the variation of the inlet cross section is 3D, with both the depth and width increasing with distance.

Most studies with a diverging channel have been conducted into horizontal channels (Akiyama and Stefan 1987; Johnson et al. 1987, 1989). In accordance with the deflection angle δ, three flow configurations may exist: (1) The flow remains attached to both sides of the wall; (2) it becomes a wall jet with a recirculation (stalled) region; or (3) it becomes a free jet with two stalled regions.

For a mildly diverging channel ($\delta < 7°$), Johnson et al. (1987) observed experimentally that the inflow remains attached to the sidewalls and the plunging process is approximately 2D. Stefan and Johnson (1989) established that the relevant independent parameters governing the distance of the plunge point x_p from the inlet are the inflow densimetric Froude number F_0, the divergence half-angle δ, and the inflow channel aspect ratio $\beta = (b_0/h_0)$ where h_0 and b_0 are the depth and the width at the entrance section of the channel.

Stefan and Johnson (1989) showed that the densimetric Froude number F_p at the plunge point is very weakly dependent on the inflow densimetric Froude number F_0. On the assumption that the mean value of F_p is 0.68, and assuming a uniform velocity and no entrainment before plunging, they derived the relation

TABLE 1. Semiempirical Relations for Depth at Plunge Point [Adapted from Akiyama and Stefan (1984)]

Authors (1)	Formula of depth at plunge point (2)
Singh and Shah (1971)	$h_p = 0.0185 + 1.3\left(\frac{q_0^2}{\varepsilon_0 g}\right)^{1/3}$ with h_p (m)
Savage and Brimberg (1975)	$h_p = \left(\frac{q_0^2}{\varepsilon_0 g F_p^2}\right)^{1/3}$ with $F_p = \frac{2.05}{1+\alpha}\left(\frac{S}{C_D}\right)^{.478}$ and $0.01 < C_D < 0.09$; $0.2 < \alpha < 0.8$
Akiyama and Stefan (1984)	Mild slope: $h_p = 1/2\{(2+\gamma)/2 + (S_2S/C_D) + \sqrt{[(2+\gamma)/2 + S_2S/C_D]^2 - 4(S_2S/C_D)/(1+\gamma)}\}(C_D/S_2S)^{1/3}\left(\frac{q_0^2}{\varepsilon_0 g}\right)^{1/3}$ Steep slope: $h_p = 1/2\{[(2+\gamma)/2 + S_1] + \sqrt{[(2+\gamma)/2 + S_1]^2 - 4(S_1)/(1+\gamma)}\}(1/S_1)^{1/3}\left(\frac{q_0^2}{\varepsilon_0 g}\right)^{1/3}$, where $S_1 h_d^2 \overline{\varepsilon_d} = \int_0^\infty \varepsilon_d z\, dz$ and $S_2 h_d \overline{\varepsilon_d} = \int_0^\infty \varepsilon_d\, dz$ with $\overline{\varepsilon_d}$ and ε_d = mean and local density excess
Stefan et al. (1988)	$h_p = \left(\frac{1}{F_p^2}\right)^{1/3}\left(\frac{q_0^2}{\varepsilon_0 g}\right)^{1/3}$ with $0.5 < F_p < 1$

J. Hydraul. Eng., 1999, 125(6): 584-594

$$\frac{x_p \tan \delta}{b_0} = 0.74\mathsf{F}_0 - 0.5 \tag{3}$$

The plunge point moves upstream as δ increases, as long as the flow remains attached.

For $\delta > 7°$ the flow separates and F_p decreases with δ, but this particular case goes beyond the scope of this paper.

Plunge Depth for Diverging Channel with Sloping Bottom

In the case of a diverging channel with a sloping bottom, the theoretical approach of the nondiverging channel, described previously, has been extended for $\delta < 7°$. It is assumed here that the plunge line is perpendicular to the main axis of the channel. In reality, the inflow moves radially downstream in the diffuser, and the plunge line is slightly curved (Johnson et al. 1987). Knowledge of the densimetric Froude number F_p allows the plunge line location to be determined. It is possible to find a relation between the depth at the plunge point h_{p1} for a channel of constant width to the depth at the plunge point h_{p2} for a diverging channel; that is

$$h_{p1} = \left(\frac{1}{\mathsf{F}_{p1}^2}\right)^{1/3} \left(\frac{q_0^2}{\varepsilon_0 g}\right)^{1/3} \tag{4a}$$

$$h_{p2} = \left(\frac{1}{\mathsf{F}_{p2}^2}\right)^{1/3} \left(\frac{q_0^2}{\varepsilon_0 g}\right)^{1/3} \left(\frac{b_0}{b_{p2}}\right)^{2/3} \tag{4b}$$

The geometric properties of the channel and a small angle of the inclination θ give

$$b_{p2} = b_0 + 2(h_{p2} - h_0) \frac{\tan \delta}{\sin \theta} \tag{5}$$

where b_{p2} = width of the channel at the plunge depth h_{p2} for a diverging channel.

Together, (4) and (5) yield

$$\frac{h_{p1}}{h_{p2}} = \left(\frac{\mathsf{F}_{p2}^2}{\mathsf{F}_{p1}^2}\right)^{1/3} \left[\frac{b_0}{b_0 + 2(h_{p2} - h_0) \dfrac{\tan \delta}{\sin \theta}}\right]^{-2/3} \tag{6}$$

Entrainment Concept

When the advancing front plunges, it disturbs and entrains the surrounding fluid. The upper boundary of the dense layer behaves like a free shear region. Turbulence at this boundary entrains the stationary ambient fluid immediately above it into the layer and dilutes it. The turbulent region grows with distance downstream as the nonturbulent fluid becomes entrained in it. This entrainment implies a flow of ambient fluid into the turbulent layer. Therefore, a small mean velocity perpendicular to the mean flow is generated when the ambient fluid is initially at rest. Ellison and Turner (1959) suggested that the velocity of the inflow into the turbulent region must be proportional to the velocity scale of the layer; the constant of proportionality is called the entrainment constant E.

Entrainment Law for Channel of Constant Width

If a 2D flow is considered and, therefore, if the lateral entrainment is neglected, the entrainment constant E is defined by the relation

$$\frac{d(UA)}{dx} = EUb_0 \tag{7}$$

where A = area of cross section of the dense layer; U = mean velocity of the layer; and b_0 = width of the layer. Entrainment is governed by the bottom slope, friction, and mixing at the free boundary of the dense layer. This mixing mechanism is parameterized by the overall Richardson number defined as

$$\mathsf{Ri} = \frac{\Delta\rho}{\rho_a} \frac{g h_d \cos \theta}{U^2} \tag{8}$$

where $\Delta\rho = \rho - \rho_a$ = local density excess with ρ, the local density; h_d = thickness of the dense layer; and θ = angle of the incline.

Ellison and Turner (1959) derived the momentum equation for a slowly varying density current with entrainment as

$$\frac{d(h_d)}{dx} = E + \frac{h_d}{3\mathsf{Ri}} \frac{d(\mathsf{Ri})}{dx} \tag{9}$$

As shown in their experiments, a short distance downstream from the source, the overall Richardson number Ri reaches a constant value Ri_n independent of x. The behavior of the underflow will be independent of the type of upstream inflow conditions and reaches its normal state. In the following discussion, this normal state is designated by the subscript n. If the flow starts too slowly, it is accelerated by gravity until Ri reaches Ri_n. If it starts too fast, increased mixing occurs until Ri_n is obtained. At this stage (i.e., normal state), there is a balance between gravity, bottom friction, and entrainment. Eq. (9) becomes

$$\frac{d(h_n)}{dx} = E_n(\mathsf{Ri}_n) \tag{10}$$

which, on integration, yields a linear growth of the density layer (Alavian and Ostrowski 1992).

Eq. (10) is only valid for a rectangular underflow. In the other case where the underflow can be approximated by a triangular shape, Fischer et al. (1979) derived the following relation for the downflow depth:

$$\frac{dh_n}{dx} = \frac{6}{5} E_n(\mathsf{Ri}_n) \tag{11}$$

The key element of these results is the functional relationship between the entrainment rate E and the Richardson number Ri. A frequently used relationship is a power law ($E = E_0 \mathsf{Ri}^{-p}$). For $\mathsf{Ri} > 2 \times 10^{-1}$, Ashida and Egashira (1975) found $E_0 = 0.0015$ and $p = 1$; Christodoulou (1986) found $E = 0.007$ and $p = 0.5$; and Parker et al. (1987) found $E_0 = 0.0028$ and $p = 1.2$ for turbidity currents. Turner (1986) showed that this functional relationship could be represented most accurately by

$$E = \frac{0.08 - 0.1\mathsf{Ri}}{1 + 5\mathsf{Ri}} \tag{12}$$

However, considering a freshwater front over a saltwater mass, Anwar (1980) observed that the variation of E with Ri cannot be described by a simple power law. Nevertheless, he showed that the coefficient of entrainment decreases rapidly as the Richardson number rises.

Entrainment Law for Diverging Channel with Sloping Bottom

An analogous study may be conducted for a diverging channel (i.e., $\delta \neq 0$) assuming, however, that the flow remains 2D ($\delta \in [0, 7°]$). Eq. (7) becomes

$$\frac{d(UA)}{dx} = EUb \tag{13}$$

where b = channel width defined as

$$b(x) = b_0 + 2x \tan \delta \tag{14}$$

Conservation of mass requires

J. Hydraul. Eng., 1999, 125(6): 584-594

$$\frac{\Delta\rho}{\rho_a} AU = \text{constant} \tag{15}$$

Combining (13) and (15) with the definition of the Richardson number [(8)] results in an expression for the entrainment as a function of the layer thickness h_d, the layer width b, and Ri

$$\frac{d(h_d)}{dx} = E + \frac{h_d}{3\text{Ri}} \frac{d(\text{Ri})}{dx} - \frac{2h_d}{3b} \frac{db}{dx} \tag{16}$$

In the case of a 3D density current, Alavian (1986) also observed that a short distance downstream of the source, Ri reaches a constant value. Assuming that the entrainment rate also reaches a constant value E_n and, then, substituting (14) into (16) yields

$$\frac{d(h_n)}{dx} = E_n - \frac{4h_n \tan\delta}{3(b_0 + 2x \tan\delta)} \tag{17}$$

k-ε MODEL OF PLUNGING DENSITY CURRENT

Equations

A 2D width-averaged density current model was implemented to analyze the kinematic behavior of a cold water release through a reservoir. This model can be used in both cases under study: (1) The constant width channel [$b(x) = b_0$]; or (2) the diverging channel [see (14)]. The standard k-ε turbulence model is adopted in the numerical model (Rodi 1984).

This model has been used for saline underflow (Fukushima and Watanabe 1990) and for buoyant vertical plane and axisymmetric jets (Sini 1986). It was shown that the k-ε model was able to explain and reproduce the mean flow properties such as the distributions of velocity, salinity, or temperature (Farrell and Stefan 1986). The considered continuity equation and momentum equations projected along the horizontal and vertical axes are

$$\frac{\partial bU}{\partial x} + \frac{\partial bW}{\partial z} = 0 \tag{18}$$

$$\frac{\partial bU}{\partial t} + \frac{\partial bUU}{\partial x} + \frac{\partial bUW}{\partial z} = b \frac{\rho - \rho_r}{\rho_r} g_1 - \frac{b}{\rho_r} \frac{\partial P}{\partial x} + \frac{\partial b(\overline{-u'u'})}{\partial x} + \frac{\partial b(\overline{-u'w'})}{\partial z} \tag{19}$$

$$\frac{\partial bW}{\partial t} + \frac{\partial bUW}{\partial x} + \frac{\partial bWW}{\partial z} = b \frac{\rho - \rho_r}{\rho_r} g_3 - \frac{b}{\rho_r} \frac{\partial P}{\partial z} + \frac{\partial b(\overline{-w'u'})}{\partial x} + \frac{\partial b(\overline{-w'w'})}{\partial z} \tag{20}$$

with

$$-\overline{u_i' u_j'} = \nu_t \left(\frac{\partial U_i}{\partial x_j} + \frac{\partial U_j}{\partial x_i} \right) - \frac{2}{3} k\delta_{ij} \tag{21}$$

and g_i, $i = 1, 3$ = projections of gravity; and δ_{ij} = Kronecker symbol.

The following assumptions are made in (19) and (20):

- Side shear stress terms that appear on the boundaries, due to the width averaging, are equal to zero, and slipping conditions are assumed.
- The dispersion terms due to lateral nonuniformities of the flow quantities, which appear in the width-averaging of the 3D equations, are neglected (ASCE 1988).

The modified k-ε model including the suitable buoyancy terms in the momentum equations and the k and ε transport equations has been implemented (Rodi 1987), where k and ε are, respectively, the width-averaged values of the turbulent kinetic energy and dissipation. The buoyancy appears in the momentum equations through the addition of the term $g_i(\rho - \rho_r)/\rho_r$ and in the k and ε equations through the addition of a term function of $B = -\nu_t g_i (1/\rho \text{Pr}(T))(\partial\rho/\partial x_i)$.

For a 2D horizontal flow of high Reynolds number, k and ε equations are, respectively

$$\frac{\partial k}{\partial t} + U \frac{\partial k}{\partial x} + W \frac{\partial k}{\partial z} = \frac{\partial}{\partial x} \left(\frac{\nu + \nu_t}{\sigma_k} \frac{\partial k}{\partial x} \right) + \frac{\partial}{\partial z} \left(\frac{\nu + \nu_t}{\sigma_k} \frac{\partial k}{\partial z} \right) + \text{Prod} + B - \varepsilon \tag{22}$$

$$\frac{\partial \varepsilon}{\partial t} + U \frac{\partial \varepsilon}{\partial x} + W \frac{\partial \varepsilon}{\partial z} = \frac{\partial}{\partial x} \left(\frac{\nu + \nu_t}{\sigma_\varepsilon} \frac{\partial \varepsilon}{\partial x} \right) + \frac{\partial}{\partial z} \left(\frac{\nu + \nu_t}{\sigma_\varepsilon} \frac{\partial \varepsilon}{\partial z} \right) + C_{1\varepsilon} \frac{\varepsilon}{k} (\text{Prod} + C_{3\varepsilon} B) - C_{2\varepsilon} \frac{\varepsilon^2}{k} \tag{23}$$

where

$$\text{Prod} = \nu_t \left[2 \left(\frac{\partial U}{\partial x} \right)^2 + \left(\frac{\partial U}{\partial z} + \frac{\partial W}{\partial x} \right)^2 + 2 \left(\frac{\partial W}{\partial z} \right)^2 \right] \tag{24}$$

where Prod = kinetic energy production drained from the mean flow and fed into the turbulent motion. The eddy viscosity $\nu_t = C_\mu (k^2/\varepsilon)$ based on k and ε is calculated by solving the two-coupled differential equations for the turbulent kinetic energy and its dissipation. Classical values of $C_{1\varepsilon}$, $C_{2\varepsilon}$, C_μ, σ_k, and σ_ε are used.

Rodi (1984) introduced $C_{3\varepsilon}$ to take the buoyancy effects into account. Numerous results show that for horizontal shear flows $C_{3\varepsilon} = 0$ and for vertical shear flows $C_{3\varepsilon} = 1$. In our case, the flow is mostly horizontal. After an optimization on the basis of experimental results (Fukushima and Watanabe 1990), a value of $C_{3\varepsilon} = 0.3$ was found. This value is in agreement with some other experiments (Farrell and Stefan 1986).

This model is more complex than the other ones (i.e., the mixing-length models or the one-equation models including a transport equation for the turbulent kinetic energy) but does not require a priori knowledge of the distribution of mixing or dissipation lengths. It is however the simplest two-equation model because it has only a few adjustment parameters.

The following equation is simultaneously solved for the heat transport:

$$\frac{\partial bT}{\partial t} + \frac{\partial bUT}{\partial x} + \frac{\partial bWT}{\partial z} = \frac{\partial}{\partial x} \left[(K + K_T) \frac{\partial bT}{\partial x} \right] + \frac{\partial}{\partial z} \left[(K + K_T) \frac{\partial bT}{\partial z} \right] \tag{25}$$

where K and K_T = molecular and turbulent heat diffusivities, respectively. K_T and ν_t are very variable within a given flow and from one flow to another, but their ratio $\text{Pr}(T) = \nu_t/K_T$ known as the turbulent Prandtl number is considered constant and is chosen equal to unity. Rodi (1987) and Fischer et al. (1979) considered that in stratified flows the turbulent Prandtl number is greater than 1 and is not really a constant, varying with stratification. This must be further investigated. Nevertheless, sensitivity analysis shows that the results are not really sensitive to the Prandtl number. Density is related to the temperature through a classical parabolic law (Henderson-Sellers 1984). An equation was simultaneously solved for a dye transport in order to follow the path of the density current.

The boundary conditions are similar to those imposed by Fukushima and Watanabe (1990). At the entrance section, profiles of velocity U_{ent} and temperature T_{ent}, k_{ent} and ε_{ent} are chosen constant with $k_{ent} = (0.1\ U_{ent})^2$ and $\varepsilon_{ent} = k_{ent}^{3/2} C_\mu^{3/4}/\kappa L$. Vertical velocity is zero, and the pressure distribution is

J. Hydraul. Eng., 1999, 125(6): 584-594

hydrostatic. κ is the von Kármán constant, and L is a characteristic length scale of the inlet depth usually taken as $0.1h_0$. At the exit section, the flow is assumed to be unidirectional so that a velocity parallel to the bottom is imposed, and the horizontal pressure gradient is chosen equal to zero.

Along the inclined wall, the classical log-law velocity distribution is applied and the turbulence is assumed to be at equilibrium

$$\frac{u_0}{u_*} = \frac{1}{\kappa} \ln\left(\frac{z_0 u_*}{\nu}\right) + A_S \tag{26}$$

$$W = 0 \tag{27}$$

$$\frac{k}{u_*^2} = \frac{1}{\sqrt{c_\mu}} \tag{28}$$

$$\varepsilon = \frac{u_*^3}{\kappa z_0} \tag{29}$$

$$\frac{\partial T}{\partial z} = 0 \tag{30}$$

where u_0 = velocity at $z = z_0$ from the wall; u_* = friction velocity at the wall; and A_S = numerical constant (=5.5 for a smooth bed).

At the water surface, the rigid lid assumption has been adopted. It implies that the free water surface is treated as a surface of symmetry for all variables. The relative error introduced by this approximation on the velocity field is of the order 10^{-3} and is not material (Farrell and Stefan 1986).

Numerical Integration

Numerical Scheme

The set of equations is solved using the numerical procedure described by Patankar (1980). It is based on a coupling between pressure and momentum (SIMPLEST algorithm) and an iterative solution procedure used here in combination with a standard k-ε closure including buoyancy. The commercially available code PHOENICS (parabolic, hyperbolic, or elliptic numerical code series) was used for calculations.

The computation method is based on a finite-volume scheme, in which the domain is divided into a series of adjacent control volumes for which a flux balance must be verified. Because diffusion and convective fluxes plus rates of change and source terms must sum to zero over each volume, the system reduces to a series of linear equations that are solved simultaneously.

The SIMPLEST algorithm iteratively adjusts an assumed pressure field by successive pressure corrections so that the resulting estimated velocity field will progressively get closer to satisfying the continuity equation. Convergence is reached when the mass imbalances in each control volume go below a threshold chosen as 0.1‰ of the cell mass.

Convective terms are discretized using the hybrid scheme described by Patankar and Spalding (1972), which consists in a centered scheme where the local Peclet number P belongs to $[-2, 2]$ and in an upwind scheme outside this interval. Unsteady terms are discretized with a fully implicit scheme that offers less constraints for the choice of the time step. Simulations start in unsteady state and proceed until a quasi-steady state is obtained. Plunging flow is intrinsically unsteady

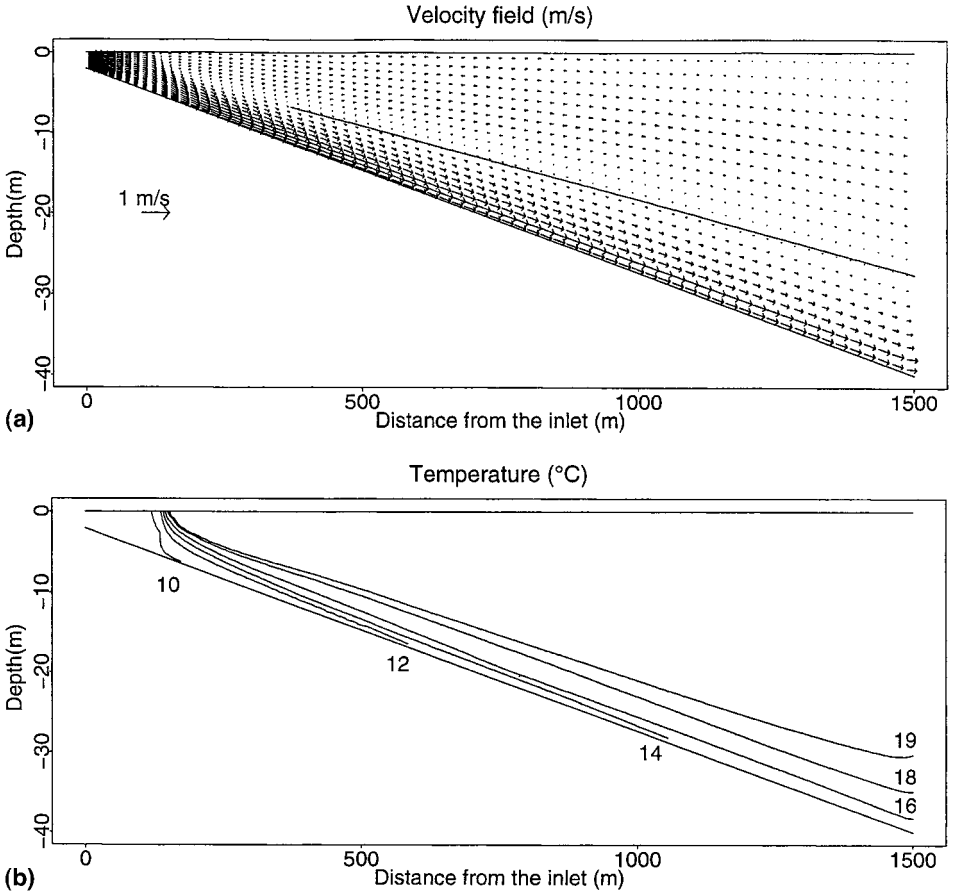

FIG. 2. (a) Velocity Field and Density Current Depth in Normal State Region Inferred from Eq. (10) (——); (b) Temperature Field for $\delta = 0°$ for $q_0 = 0.75$ m²/s (Elapsed Time = 5 h)

because of continuous entrainment of ambient water (Farrell and Stefan 1988). For the diverging case, the varying width of the channel is taken into account through the integration process over finite volumes.

Implementation

Calculations have been conducted in a domain containing 70 × 20 cells in the *x*- and *z*-direction using a body-fitted coordinated grid. The advantage of this method is that the directions of the cell boundaries are aligned with the domain contour. With such a grid, however, equations are not solved in a Cartesian coordinate system but in a local coordinate system. Dimensions of the grid are characteristic of environmental scales (i.e., 1,500 m × 40 m) in the *x*-*z*-directions. Cells are unevenly spaced, and the grid is squeezed upstream and near the bottom where shear stress occurs and velocity gradients develop. To avoid ''zig-zag'' pressure fields described by Patankar (1980), a staggered grid was employed. The choice of the mesh characteristics was established after several refinements were tested [i.e., regular and irregular grids of the following sizes: 40 × 10 (Grid 1), 70 × 20 (Grid 2), and 100 × 40 (Grid 3)]. Regular grids were not adapted due to their coarseness in the plunging region. For irregular grids, however, the plunge point location was far downstream for Grid 1, whereas results were similar for Grids 2 and 3 [see Farrell and Stefan (1986)]. As a result, Grid 2 was chosen for time calculation economy. Parameters values used in the calculation were $S = 0.025$, $h_0 = 2$ m, $b_0 = 20$ m, and $\varepsilon_0 = 1.5\ 10^{-3}$ (Fig. 1). For the constant width channel, several specific flow conditions, $q_0 = 0.75$, 1.5, 2.25, 3, and 3.75 m^2/s, were used. For the diverging channel, $q_0 = 0.75$ m^2/s was used. A time step of 6 min was adopted. According to the classification proposed by Akiyama and Stefan (1984), the slope used for the calculations must be considered as a steep slope.

RESULTS

Numerical results derived from the *k*-ε model are compared with semiempirical models for both constant width and diverging channels. Figs. 2 and 3 present numerical results both for a constant with channel ($q_0 = 0.75$ m^2/s) and for a diverging channel ($q_0 = 0.75$ m^2/s, $\delta = 7°$). As the density current front advances, a recirculating flow is set up just above and leads to a well-defined convergence zone at the plunge point. Comparisons between the two cases clearly shows that the divergence leads to a displacement of the plunge point upstream and to a reduction of the density current thickness.

Estimation of Macroscopic Parameters from Numerical Results

Estimation of Density Current Thickness h_d

Density current thickness h_d was estimated by adding the cells' thicknesses where the horizontal velocity is positive and where the dye concentration is >1% C_0, with C_0 being the dye concentration at the inlet. This definition allows the calculation of the averaged velocity $\bar{U}$ of the density current in a given cross section. Moreover, the depth of plunging h_p is the value of h_d where the flow begins to plunge and leaves the surface.

Estimation of Entrainment E

Integrating (13) between two adjacent cross sections leads to the following relation for the entrainment:

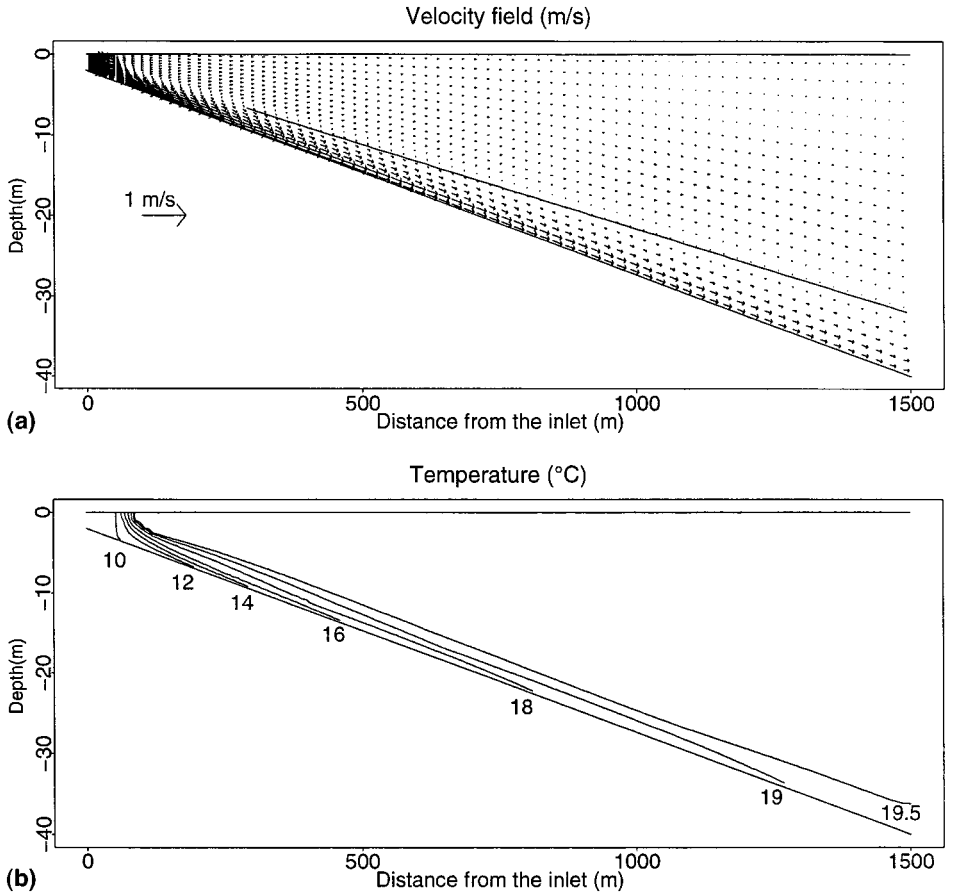

FIG. 3. (a) Velocity Field and Density Current Depth in Normal State Region Inferred from Eq. (17) (——); (b) Temperature Field for $\delta = 7°$ for $q_0 = 0.75$ m^2/s (Elapsed Time = 13 h)

J. Hydraul. Eng., 1999, 125(6): 584-594

$$E = \frac{1}{\overline{Ub}} \frac{\Delta Q}{\Delta x} \tag{31}$$

where Δx = distance; ΔQ = density current flow variation; and b = averaged width of the channel between the two sections.

Estimation of Richardson Number Ri

Ri is estimated by the following relation:

$$\text{Ri} = \frac{(\overline{\rho_d} - \rho_{surf})}{\rho_{surf}} \frac{g(\overline{h_d})\cos\theta}{U^2} \tag{32}$$

where $\overline{\rho_d}$ = mean density of the bottom current; and ρ_{surf} = density of water at the surface that is taken equal to ρ_a downstream of the plunge point.

Channel of Constant Width

Thickness of Bottom Current

Fig. 4 shows the evolution of the depth of the bottom current along the x-axis. Larger values of h_d occur at the plunge point. As only discrete values for h_d depending on the grid were calculated, results were smoothed. From the inlet, h_d increases linearly according to the bottom slope and decreases abruptly at the plunge point. Then, after a transition zone, another linear behavior is observed, due to the entrainment, which constitutes the normal state region.

Fig. 5 indicates that numerical results coincide with most of the semiempirical relations for the plunge depth. In particular, the expression suggested by Akiyama and Stefan (1984) that takes into account the nonuniformity of density over depth is closer to the numerical results. For this study we have chosen values of S_1 covering the range [0.2, 0.3] obtained by Ellison and Turner (1959) for bounded currents and Alavian (1986) for unbounded currents. Schläpfer et al. (1987), however, obtained S_1 = [0.6, 1] from measured velocity profiles in a mildly sloped channel.

Entrainment

Vertical velocity distributions allow the determination of the entrainment coefficient [(31)]. For the various flow conditions, it was found to range from 0.006 to 0.022. For each flow condition, E varies with x; larger values occur at the plunge point due to entrance effects and initial mixing or to the hydraulic instability that occurs downstream of the plunge line. In Lake Mead, Fischer and Smith (1983) observed that half of the entrainment occurs at the plunge point, which is qualitatively confirmed here by the higher values found numerically at that point. In Lake Lucerne, Wüest et al. (1988) found values of E within the range of 0.02−0.1 at the plunge point.

After the plunge point, the value of the entrainment converges toward ≃0.008 [(31)] as the flow reaches the normal state. This value seems to be independent of the inflow rate q_0. Moreover, this value lies in the range of 0.007−0.009 for

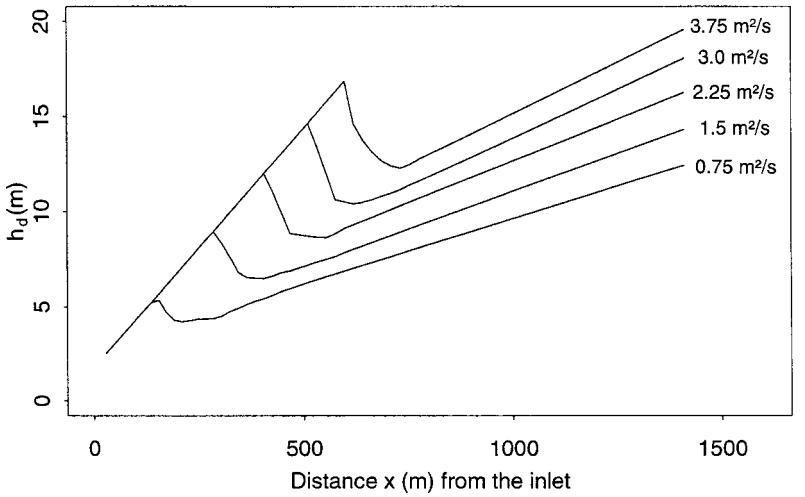

FIG. 4. Dependence of h_d on x. Figures Refer to Inflow Rate per Unit Width q_0

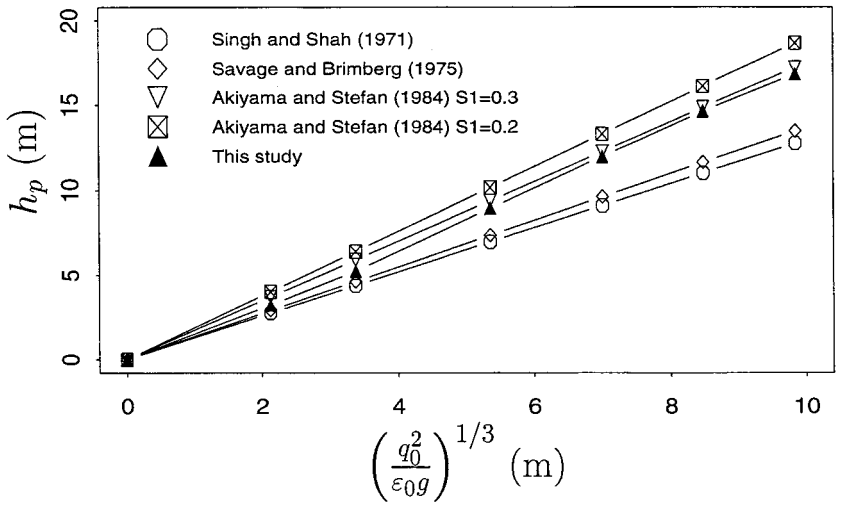

FIG. 5. Comparison of Model Results with Equations for Plunge Depth

J. Hydraul. Eng., 1999, 125(6): 584-594

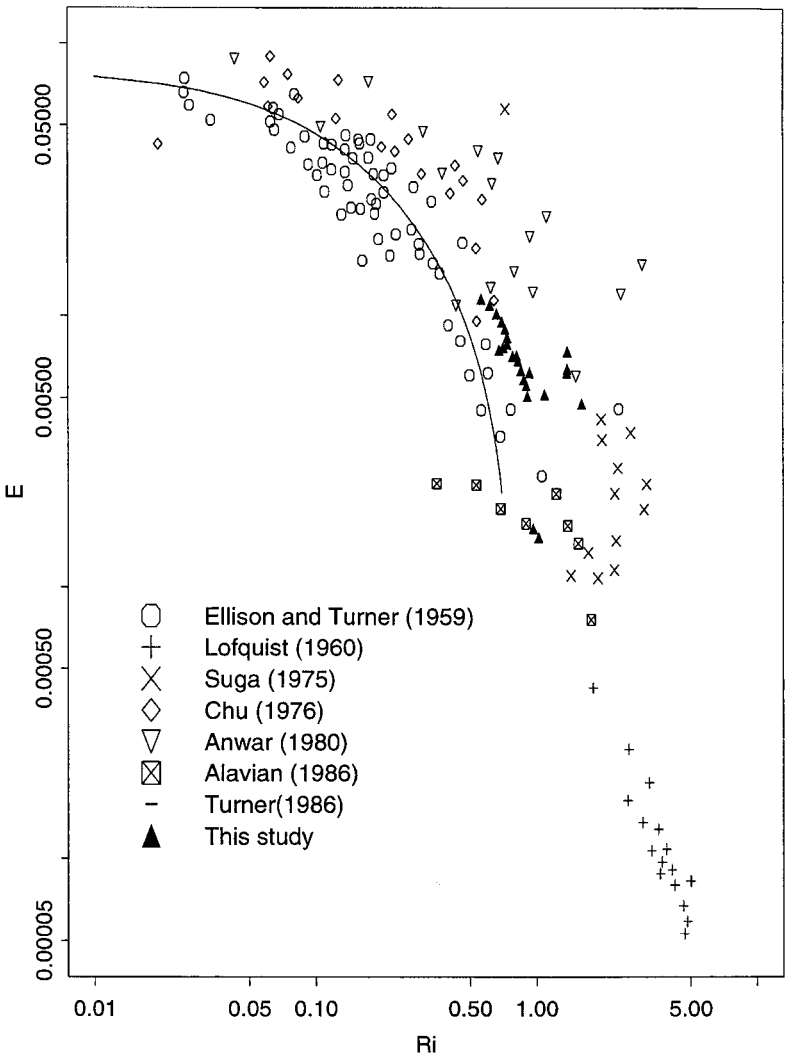

FIG. 6. Dependence of Entrainment Coefficient on Richardson Number $E = E(\mathrm{Ri})$ [Adapted from Alavian (1986) and Anwar (1980)]

the slope of $h_d(x)$ (Fig. 4) in the normal state region. From (10) this slope equals the entrainment coefficient in the normal state region.

In the normal state region, the thickness of the bottom current is reported in Fig. 2. It was estimated using the following procedure:

1. One point belonging to the h_d line, far beyond the plunge point and the transition zone, is calculated from the numerical results. (It is estimated by adding the cells' thicknesses where the horizontal velocity is positive and where the dye concentration is $>1\%C_0$, with C_0 being the dye concentration at the inlet.)
2. Then E_n is calculated using (31).
3. Finally, the straight line in Fig. 2(a) is inferred from the preceding values and from (10).

Richardson Number

It is possible to infer the dependence of the entrainment coefficient on the Richardson number. E plotted against the normal Richardson number is depicted in Fig. 6. Also plotted are data from the experiments of Ellison and Turner (1959), Lofquist (1960), Alavian (1986), and Anwar (1980), as well as the empirical formula established by Turner (1986). The range of numerical values of E and Ri is quite narrow but falls exactly in the middle of the data obtained by Ellison and Turner and Anwar. E is very sensitive to Ri, particularly in the range of the Ri values tested that correspond to the case of a river entering a lake.

Diverging Channel with Sloping Bottom

The effect of the divergence angle δ on the plunge depth is depicted in Fig. 7, where h_{p2} is plotted as a function of h_{p1}. Points correspond to numerical results, and solid lines show the best adjustment of (6) on these points on the basis of a least-square criterion. This enables the calculation of the ratio $\mathrm{F}_{p2}/\mathrm{F}_{p1}$. Both the k-ε numerical model and the analytical model [(6)] are in good agreement.

For a given flow rate, the plunge depth decreases with an increase of the divergence angle δ. For example, when δ varies from 0 to 1°, for a flow of 3 m^2/s, the plunge depth moves from 15 to 11 m. Thus, taking into account the divergence angle in simulation of density currents is of primary importance.

Fig. 8 depicts the relation between $\mathrm{F}_{p2}/\mathrm{F}_{p1}$ and δ. We find values of $\mathrm{F}_{p2}/\mathrm{F}_{p1}$ increasing from 1 to 1.26 with δ increasing from 0 to 7°. In our case ($S = 0.0025$), a linear fit between $\mathrm{F}_{p2}/\mathrm{F}_{p1}$ and δ can be found

$$\frac{\mathrm{F}_{p2}}{\mathrm{F}_{p1}} = 1 + 0.04\delta \tag{33}$$

J. Hydraul. Eng., 1999, 125(6): 584-594

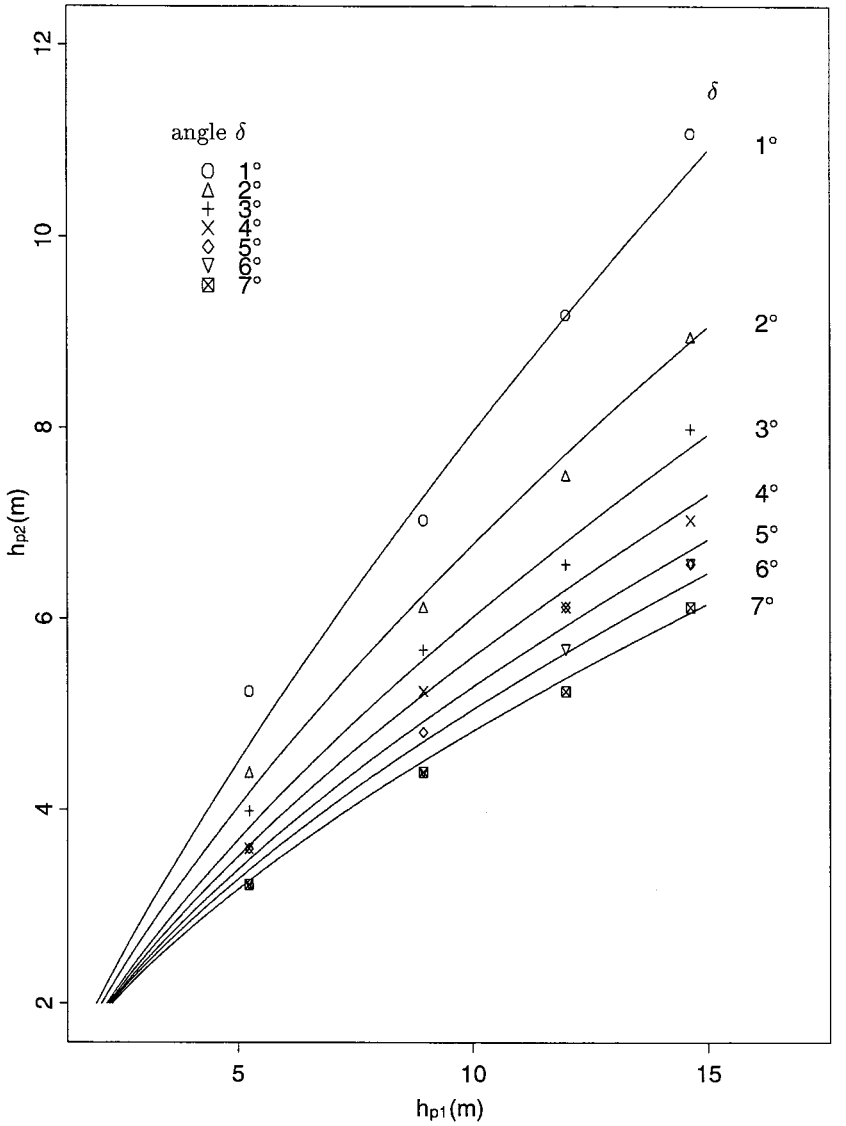

FIG. 7. Relationship between h_{p1} and h_{p2} for $\delta \in [1, 7°]$. Solid lines (——) correspond to Eq. (4) and Points to Numerical Results

with δ varying between 0 and 7°. Such results confirm experimental data from Akiyama and Stefan (1987) that clearly show that the densimetric Froude number F_{p2} grows with the channel divergence angle. It should be noted however that (33) is valid for the slope (i.e., $S = 0.025$) considered here and should therefore not be considered as universal.

Entrainment calculated on the basis of the numerical results using (31) leads again to a constant value of $E_n = 0.008$ in the normal state region. E_n appears independent of δ with angles varying between 0 and 7°.

The thickness of the bottom density current is drawn in Fig. 3(a). It is calculated with the procedure described in the constant width channel case but using (17) instead of (10). Despite the fact that (17) is nonlinear in the normal state region, Fig. 3 shows that a good linear approximation is acceptable. Nonlinearities for small angles ($\delta < 7°$) remain insignificant; the second part of the right side of this equation is negligible.

CONCLUSIONS

The 2D density currents on a sloping bottom with and without divergence effects have been investigated theoretically and numerically. Globally, the k-ε with buoyancy effects model appears to be able to reproduce the integral properties of density currents, summarized as follows:

- The k-ε model provides a good approximation for the calculation of the plunge point location in a sloping channel of constant width. The slope of the line $h_p = f((q_0^2/\varepsilon_0 g)^{1/3})$ is in good agreement with several empirical formulas reported.
- The values of E obtained for various q_0 are in the same range as those obtained experimentally by many authors. Theories of two-layer systems are in agreement with the numerical results. In particular, the linear growth of the density layer downstream of the plunge point in the normal state region with the distance from the inlet has been underlined. Moreover, for the diverging channel, E_n appears to be independent of δ.
- A relation between the depth at the plunge point for a constant width channel and that for a diverging channel with sloping bottom has been established and verified numerically. In addition, an expression for the normal depth h_n following plunging has been established and compared with the model. For small diverging angles, nonlinearities in this expression remain negligible.

However, field studies and laboratory experiments will be needed to gain more understanding of the mechanisms driving density currents. The experiments should be conducted with the aim of measuring the mean properties of the flow and the

J. Hydraul. Eng., 1999, 125(6): 584-594

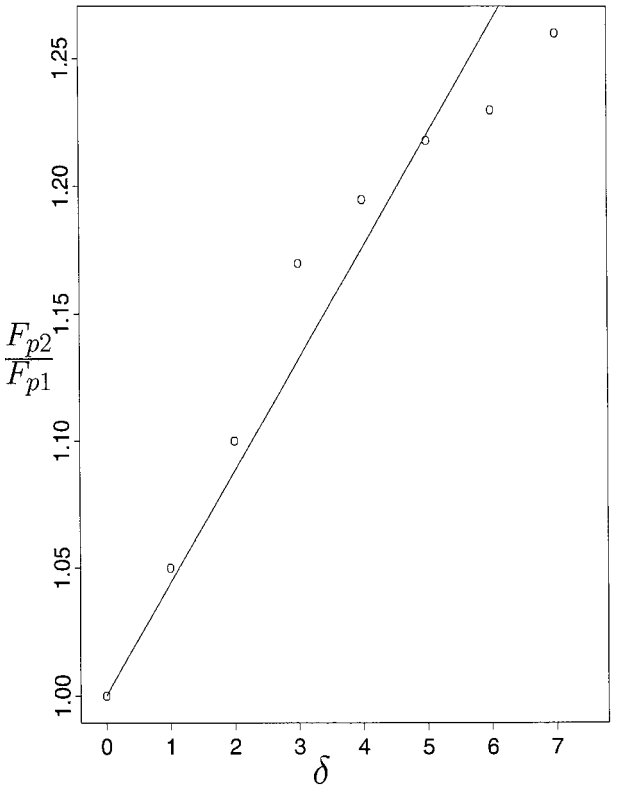

FIG. 8. Values of Ratio of F_{p1}/F_{p2} Utilized in Fig. 7 and Corresponding Adjustment Law for $\delta \in [1, 7°]$

local structures to gain a better understanding of the turbulent mixing properties. Insight and data obtained from such experiments are essential in model formulation and as inputs to models. Furthermore, the linkage of density current models to models for overall lake/reservoir (i.e., water quality models) should be improved.

ACKNOWLEDGMENTS

This study was supported by the French Ministry of Agriculture. The writers wish to thank the Institute of Fluid Mechanics, Toulouse, France, for providing computer facilities.

APPENDIX I. REFERENCES

Akiyama, J., and Stefan, H. G. (1984). ''Plunging flow into a reservoir.'' *J. Hydr. Engrg.*, ASCE, 110, 484–499.
Akiyama, J., and Stefan, G. (1987). ''Onset of underflow in slightly diverging channels.'' *J. Hydr. Engrg.*, ASCE, 113, 825–844.
Alavian, V., Jirka, G. H., Denton, R. A., Johnson, M. C., and Stefan, H. G. (1992). ''Density currents entering lakes and reservoirs.'' *J. Hydr. Engrg.*, ASCE, 118, 1464–1489.
Alavian, V., and Ostrowski, J. (1992). ''Use of density current to modify thermal structure of TVA reservoirs.'' *J. Hydr. Engrg.*, ASCE, 106, 39–55.
Alavian, V. (1986). ''Behavior of density current on an incline.'' *J. Hydr. Engrg.*, ASCE, 112, 27–42.
Anwar, H. O. (1980). ''Measurements on entrainment through a front.'' *Proc., 2nd Int. Symp. on Stratified Flows*, Norwegian Institute of Technology, Trondheim, Norway, 143–153.
ASCE Task Committee on Turbulence Models in Hydraulic Computations. (1988). ''Turbulent modeling of surface water flow and transport: Part 1.'' *J. Hydr. Engrg.*, ASCE, 114(9), 970–991.
Ashida, K., and Egashira, S. (1975). ''Basic study on turbidity currents.'' *Proc., Jap. Soc. Civ. Engrg.*, Tokyo, 237, 37–50.
Buchak, E., and Edinger, J. (1984). ''Simulation of density underflow into Wellington reservoir using longitudinal-vertical hydrodynamics.'' *Tech. Rep. No. 84/18/R*, J. E. Edinger Associates, Wayne, Pa.
Carmack, E. C., Pharo, C. H., and Daley, R. J. (1979). ''Importance of lake-river interaction on seasonal patterns in the general circulation of Kamloops Lake, British Columbia.'' *Limnol. Oceanogr.*, 21, 634–644.
Carmack, E. C., Wiegand, R. C., Daley, R. J., Gray, B. J., Jasper, S., and Pharo, C. H. (1986). ''Mechanisms influencing the circulation and distribution of water mass in a medium residence-time lake.'' *Limnol. Oceanogr.*, 31, 249–265.
Chikita, K. (1992). ''The role of sediment-laden underflows in lake sedimentation: Glacier-Fed Peyto Lake, Canada.'' *J. Fac. Sco. Hokkaido Univ.*, 9, 211–224.
Christodoulou, G. (1986). ''Interfacial mixing in stratified flows.'' *J. Hydr. Res.*, Delft, The Netherlands, 24, 77–92.
Chu, V. H., and Vanvari, M. R. (1976). ''Experimental study of turbulent stratified shearing flow.' *J. Hydr. Div.*, ASCE, 102(6), 691–706.
Denton, R. A. (1985). ''Density current inflows to run of the river reservoirs.'' *Proc., 21st IAHR Congr.*
Ellison, T. H., and Turner, J. S. (1959). ''Turbulent entrainment in stratified flows.'' *J. Fluid Mech.*, Cambridge, England, 6, 423–448.
Farrell, G., and Stefan, H. (1988). ''Mathematical modeling of plunging reservoir flows.'' *J. Hydr. Res.*, Delft, The Netherlands, 26, 525–537.
Farrell, G., and Stefan, H. (1986). ''Buoyancy induced plunging flow into reservoirs and coastal regions.'' *Tech. Rep. No. 241*, St. Anthony Falls Hydr. Lab., University of Minnesota, Minneapolis.
Fischer, H. B., List, E. J., Koh, R. C. Y., Imberger, J., and Brooks, N. H. (1979). *Mixing in inland and coastal waters*. Academic, New York.
Fischer, H. B., and Smith, R. D. (1983). ''Observation of transport to surface waters from a plunging inflow to Lake Mead.'' *Limnol. Oceanogr.*, 28, 258–272.
Fukushima, Y., and Watanabe, M. (1990). ''Numerical simulation of density underflow by the *k*-ε turbulence model.'' *J. Hydrosci. Hydr. Engrg.*, 8, 31–40.
Hamblin, P. F., and Carmack, E. C. (1978). ''River induced currents in a fjord lake.'' *J. Geophys. Res.*, 83, 885–899.
Hauenstein, W., and Dracos, T. (1984). ''Investigation of plunging density currents generated by inflows in lakes.'' *J. Hydr. Res.*, Delft, The Netherlands, 22, 157–179.
Hebbert, B., Imberger, J., Loh, I., and Patterson, J. (1979). ''Collie river underflow into the Wellington reservoir.'' *J. Hydr. Div.*, ASCE, 106, 533–545.
Henderson-Sellers, B. (1984). *Engineering limnology*. Pitman Advanced Publishing Program, London.
Imberger, J., and Patterson, J. (1981). ''A dynamic reservoir simulation model—DYRESM:5.'' *Transport models for inlands and coastal waters*, Academic, New York, 310–360.
Johnson, T., Ellis, C., and Stefan, H. (1989). ''Negatively buoyant flow in diverging channel. IV: Entrainment and dilution.'' *J. Hydr. Engrg.*, ASCE, 115, 437–456.
Johnson, T., Farrell, G., Ellis, C., and Stefan, H. (1987). ''Negatively buoyant flow in a diverging channel. I: Flow regimes.'' *J. Hydr. Engrg.*, ASCE, 113, 716–730.
Jokela, J., and Patterson, J. (1985). ''Quasi-two-dimensional modelling of reservoir inflow.'' *Proc., 21st IAHR Congr*.
Kranenburg, C. (1993). ''Gravity-current fronts advancing into horizontal ambient flow.'' *J. Hydr. Engrg.*, ASCE, 119, 369–379.
Lofquist, K. (1960). ''Flow and stress near an interface between stratified liquids.'' *Phys. of Fluid*, 3, 72–182.
Parker, G., Garcia, M., Fukushima, M., and Yu, W. (1987). ''Experiments on turbidity currents over an erodable bed.'' *J. Hydr. Res.*, Delft, The Netherlands, 25, 123–147.
Patankar, S. (1980). *Numerical heat transfer and fluid flow*. McGraw-Hill, New York.
Patankar, S., and Spalding, D. (1972). ''A calculation procedure for heat, mass and momentum transfer in three-dimensional parabolic flows.'' *J. Heat Mass Transfer*, 15, 1787.
Rodi, W. (1984). *Turbulence models and their application in hydraulics: A state of the art review*. IAHR, Delft, The Netherlands.
Rodi, W. (1987). ''Examples of calculation methods for flow and mixing in stratified fluids.'' *J. Geophys. Res.*, 92, 5305–5328.
Savage, S. B., and Brimberg, J. (1975). ''Analysis of plunging phenomena in water reservoirs.'' *J. Hydr. Res.*, Delft, The Netherlands, 13, 187–205.
Schläpfer, D. B., Bühler, J., and Dracos, T. (1987). ''Dense inflows into narrow reservoirs.'' *Proc., 3rd Int. Symp. on Stratified Flows*.
Serruya, S. (1974). ''The mixing patterns of the Jordon River in Lake Kinneret.'' *Limnol. Oceanogr.*, 19, 175–181.
Singh, B., and Shah, C. R. (1971). ''Plunging phenomenon of density currents in reservoirs.'' *La Houille Blanche*, Paris, 1, 59–64.
Sini, J. F. (1986). *Modélisation d'écoulements turbulents libres bidimensionnels avec effets de flottabilité—cas du panache en milieu stratifié*. PhD thesis, Université d'Aix-Marseille IL, Aix-Marseille, France, (in French).
Smith, P. C. (1975). ''A stream tube model for bottom boundary currents in the ocean.'' *Deep Sea Res.*, 22, 853–873.
Stefan, H., and Johnson, T. (1989). ''Negatively buoyant flow in diverging

channel. III: Onset of underflow.'' *J. Hydr. Engrg.*, ASCE, 115, 423–436.
Stefan, H. G., Johnson, T. R., Ellis, C. R., Farell, G. J., and Akiyama, J. (1988). ''Physical limnology, laboratory studies on the initiation of density currents by inflows to lakes and reservoirs.'' *Verhandlungen Internationale Vereinigung für Theoritische und Angewandte Limnologie*, Stuttgart, Germany, 23, 58–61.
Suga, K. (1975). ''Salt wedge intrusion with entrainment.'' *Proc., IAHR*, International Association for Hydraulic Research, Delft, The Netherlands, 172–179.
Turner, J. (1986). ''Turbulent entrainment: The development of the entrainment assumption, and its application to geophysical flows.'' *J. Fluid Mech.*, Cambridge, England, 173, 431–471.
Wüest, A., Imboden, D. M., and Schurter, M. (1988). ''Origin and size of hypolimnic mixing in Urnersee, the southern basin of Vierwaldstattersee (lake Lucerne).'' *Sweizeirische Zeitschrift für Hydrologie*, 50(1), 40–70.

APPENDIX II. NOTATION

The following symbols are used in this paper:

A = cross section of dense layer;
A_S = numerical constant dependent on bottom roughness;
$\bar{b}$ = averaged width channel between two cross sections;
b_{p2} = width of channel at plunge point (diverging channel);
$b(x)$ = width of channel at x;
b_0 = width of inflow channel;
C_D = total friction coefficient;
C_0 = dye concentration at inlet;
$C_{1\varepsilon}$, $C_{2\varepsilon}$, $C_{3\varepsilon}$, $C\mu$ = constants of k-ε model;
E = entrainment rate;
E_n = entrainment rate in normal state;
F_p = densimetric Froude number at plunging;
F_{p1} = densimetric Froude number at plunging (constant width channel);
F_{p2} = densimetric Froude number at plunging (diverging channel);
F_0 = inflow densimetric Froude number;
g = acceleration of gravity;
g_i = component of acceleration of gravity;
h = thickness of dense layer;
$\underline{h_d}$ = thickness of bottom current;
$\overline{h_d}$ = averaged thickness of bottom current between two cross sections;
h_n = thickness of bottom current in normal state;
h_p = depth of plunging;
h_{p1} = depth of plunging (constant width channel);
h_{p2} = depth of plunging (diverging channel);
h_0 = depth of inflow channel;
K = molecular heat diffusivity;
K_T = turbulent heat diffusivity;
k = turbulent kinetic energy (width-averaged);
k_{ent} = inlet turbulent kinetic energy (width-averaged);
L = characteristic length scale;
P = pressure;
$\mathsf{Pr}(T)$ = Prandtl number of temperature;
Q = flow rate;
q_p = flow rate per unit width at plunging;
q_0 = inflow rate per unit width;
Ri = overall Richardson number;
Ri_n = normal Richardson number;
S = slope;
S_1, S_2 = shape factors due to nonuniformity of density profile;
T = temperature;
T_{ent} = inlet temperature;
$\overline{U}$ = averaged U-velocity between two cross sections;
U, W = width-averaged velocities along x- and z-directions;
U_{ent} = velocity in inlet section;
u', w' = velocity fluctuations along x- and z-directions;
u_0 = velocity at distance $z = z_0$ from bottom;
u_* = bottom friction velocity;
x, z = coordinate directions;
x_n = abscissa coordinate in normal state;
x_p = distance to plunge point;
z_0 = distance of first cell from wall;
β = b_0/h_0 aspect ratio;
γ = initial mixing;
$\Delta\rho_0$ = $\rho_0 - \rho_a$;
δ = divergence half-angle of channel;
ε = dissipation (width-averaged);
ε_{ent} = inflow dissipation;
ε_0 = $\Delta\rho_0/\rho_n$;
θ = angle of incline;
κ = von Kármán constant;
ν = kinematic viscosity;
ν_t = turbulent kinematic viscosity;
ρ = local density;
ρ_a = density of ambient water;
$\underline{\rho_d}$ = local density of bottom current;
$\overline{\rho_d}$ = averaged density of bottom current between two cross sections;
ρ_{surf} = density at surface;
ρ_0 = density of inflow; and
$\sigma_{k,\varepsilon}$ = turbulent Schmidt number for k and ε.